

A grand-design spiral galaxy 1.5 billion years after the Big Bang with JWST

Rashi Jain^{1,*}, Yogesh Wadadekar¹

National Centre for Radio Astrophysics - Tata Institute of Fundamental Research, Post Bag 3, Ganeshkhind, Pune 411007, India

ABSTRACT

We report the discovery of a large (~ 10 kpc diameter), massive ($\log(M_*/M_\odot) = 10.15 \pm_{-0.01}^{+0.01}$), grand-design spiral galaxy with photometric redshift $z_{\text{phot}} = 4.03$ in the UNCOVER and Medium band, Mega Science surveys with JWST. This is the highest redshift spiral galaxy discovered with JWST, so far. In the rest-frame near-UV and far-UV, we clearly see the beads-on-a-string pattern of star formation; in the rest-frame visible bands, each string appears as an arm. Spectral energy distribution modeling using the Bagpipes code is strongly constrained by detections and flux measurements in 21 JWST and HST filters. The stellar mass-weighted age is 228 Myr, implying 50% of the stars in the galaxy formed after $z \sim 4.5$. This is a highly star-forming galaxy (SFR of $57.57 \pm_{-1.90}^{+1.80} M_\odot \text{ yr}^{-1}$). We detect strong H- α + [NII] emission from the entire disk. Detection of a spiral galaxy at $z \sim 4$ indicates that massive and large spiral galaxies and disks were already in place merely 1.5 billion years after the Big Bang.

Key words. galaxies: spiral – galaxies: formation – galaxies: evolution – galaxies: high-redshift

1. Introduction

Spiral arms are the primary distinguishing feature of the majority of disk galaxies in the nearby Universe. Spiral galaxies come in different flavors, ranging from grand-design and multi-arm spiral galaxies with prominent arms to flocculent spiral galaxies having rather small or patchy arms (Elmegreen & Elmegreen 2014). Several theories have been developed to explain the origin, longevity, and structure of spiral arms. Quasi-Steady-State Density Wave theory (Lin & Shu 1964) and swing amplification of local gravitational instabilities (Toomre 1977, 1981) are two of the most popular theories for the origin of spiral arms in disk galaxies.

It is still not completely clear when and how spiral galaxies first emerged in the early Universe. Using observations with the Hubble Space Telescope (HST), we know that disk galaxies, and thus by extension spiral galaxies, become increasingly rare in the high redshift Universe. The rarity of high redshift spirals might be a consequence of galaxies being dynamically hot at those early epochs. Dynamically hot systems tend to form clumpy structures, whereas cold disks with low velocity dispersion are required to form spiral arms (Genzel et al. 2006; Sellwood 2014). Cosmological dimming, morphological k-correction (Rawat et al. 2009) and observational constraints may also play a role in the observed rarity of high redshift spirals. As redshift increases, it becomes increasingly difficult to identify and study the spiral pattern in galactic disks due to the limitations of sensitivity and resolution. Even with the deepest HST observations, studies of spiral galaxies were limited to $z < 3$. A study of spiral galaxies in the CANDELS field by Margalef-Bentabol et al. (2022), suggests that the spiral galaxy fraction decreases monotonically with redshift. Using HST data, only two spiral galaxies have been discovered at a redshift of $z > 2$ (Law et al. 2012; Yuan et al. 2017).

James Webb Space Telescope (JWST)'s unprecedented sensitivity and resolution in the observed frame near-infrared (NIR) that provides access to the optical rest frame at redshifts higher than 3, has made it possible to detect spiral galaxies at these redshifts for the first time. With JWST, astronomers have discovered a significant population of disk galaxies at high redshifts ($z > 3$) (Kartaltepe et al. 2023; Ferreira et al. 2022; Ferreira et al. 2023; Robertson et al. 2023; Nelson et al. 2023; Jacobs et al. 2023). The discovery of high redshift disk galaxies poses challenges to our current understanding of galaxy formation (Kartaltepe et al. 2023; Labbé et al. 2023). JWST's sensitivity also allows us to detect spiral features in the high redshift disk galaxies. Recently using JWST observations, few studies such as Wu et al. (2022), Fudamoto et al. (2022), and Costantin et al. (2023) have discovered individual spiral galaxies at high redshifts of 3.06, 2.463 and 3.03 respectively. Another study by Kuhn et al. (2024) finds that the observed spiral galaxy fraction decreases from 46 % at $z \sim 1$ to 4% at the redshifts of $z \sim 3$. If this trend continues, the fraction may be even lower at higher redshifts. Using an extrapolation method of artificially redshifting spiral galaxies to high redshifts and Kuhn et al. (2024) claim that the intrinsic fraction of spiral galaxies should be $\sim 25\%$ at the redshifts of $z \sim 3$. There is a clear mismatch between the observed fraction and the prediction, likely due to observational biases in detection. It is therefore crucial to discover as many spiral galaxies at high redshifts, as possible. Even with JWST observations, only a few individual spiral galaxies have been found at $z \sim 3$, although the number of disk galaxies discovered is considerably larger.

In a few complementary studies, astronomers have also discovered spiral structures in galactic disks at comparably high redshifts through ground-based observations using ALMA (Tsukui & Iguchi 2021; Tsukui et al. 2024; Huang et al. 2023). A study by (Tsukui & Iguchi 2021; Tsukui et al. 2024) has reported the discovery of spiral structure at a high redshift of $z \sim 4$ through submm ALMA observations. However, the HST image of this ALMA detected galaxy does not show a spiral structure

* e-mail: rjain@ncra.tifr.res.in

as its observer frame optical light is dominated by the quasar at the center of the galaxy (Tsukui et al. 2023). Due to the presence of the quasar, it is not possible to confirm whether the spiral arms in the ALMA detected Tsukui’s galaxy are stellar arms.

In this paper, we present the discovery, in the Abell 2744 cluster field, of a two-armed, grand-design spiral galaxy, with a redshift of $z \sim 4$, when the Universe was only ~ 1.5 billion years old. Since this is a grand design spiral (GDSp) galaxy lying in the A2744 field at $z \sim 4$, we designate it as A2744-GDSp-z4. A2744-GDSp-z4 is a massive (stellar mass $\sim 10^{10.15} M_{\odot}$) and highly star forming galaxy with a star formation rate (SFR) of $\sim 58 M_{\odot} \text{ yr}^{-1}$ making it analogous to starburst spiral galaxies in the nearby Universe. It is the most distant spiral galaxy discovered by JWST, so far.

In Section 2, we describe the UNCOVER dataset. In Section 3 we discuss our methods for SED modeling and quantitative parametric and non-parametric measures of galaxy morphology. In Section 4, we provide a discussion of our results and interpret the possible consequences of this discovery on models of high redshift spiral galaxy formation. Throughout, we assume a standard cosmological model with $\Omega_M = 0.3$, $\Omega_{\Lambda} = 0.7$ and Hubble’s constant $H_0 = 70 \text{ km s}^{-1} \text{ Mpc}^{-1}$.

2. Dataset

We utilise the publicly available JWST and HST data from the ULTRADEEP NIRSPEC AND NIRCAM OBSERVATIONS BEFORE THE EPOCH OF REIONIZATION (UNCOVER) survey Data Release 3 (Bezanson et al. 2022; Weaver et al. 2024; Suess et al. 2024) in the Abell 2744 field. The UNCOVER DR3 dataset includes photometry and deep mosaics in a total of 15 JWST/NIRCam (F090W, F115W, F150W, F200W, F277W, F356W, F410M, F444W), HST/ACS (F435W, F606W, F814W), and HST/WFC3 (F105W, F125W, F140W, F160W) filters. It also includes additional observations from the Medium bands Mega Science survey in 11 additional medium band filters (F140M, F162M, F182M, F210M, F250M, F300M, F335M, F360M, F430M, F460M, F480M) and the two shortest wavelength broad-band filters (F070W and F090W). The addition of data in a large set of medium-band filters through the Mega Science observations, enables the correct disentangling of the relative contribution of line and continuum emission to broad-band photometry, leading to non-degenerate photometric redshifts and accurate stellar population synthesis modeling. Detailed comparisons of photometric and spectroscopic redshifts presented in Suess et al. (2024) show that the number of catastrophic outliers is small, and an overwhelming majority of the outliers have a higher spectroscopic redshift than their photometric redshift. The UNCOVER DR3 SUPER catalog provides photometry for over 70,000 objects over an area of 56.2 arcmin^2 . Over the limited area of overlap between the UNCOVER and Medium Band Mega Science surveys, the UNCOVER DR3 datasets include observations in all NIRCam medium and broad-band filters. The DR3 dataset includes image mosaics that are astrometrically matched and pixel aligned with a pixel scale of $0.02 \text{ arcsec/pixel}$ in the short wavelength filters (with wavelength less than that of F250W) and $0.04 \text{ arcsec/pixel}$ in the long wavelength (F250W and longer wavelength) filters. As value additions, the DR3 release also provides photometric redshifts derived via the stellar population synthesis (SPS) codes Prospector (Johnson et al. 2021) by Wang et al. (2024) and EAZY (Brammer et al. 2008)). Abell 2744 is a massive galaxy cluster that magnifies the background galaxies upto dozens of times through gravitational lensing. The DR3 catalog also supplies us with the strong lensing

magnification of each object derived via an updated version of the mass model described in Furtak et al. (2023). In DR4 of UNCOVER, the strong lensing magnifications have been further updated. We use these latest magnifications in our analysis. In this work, we perform SED modeling using Bagpipes and EAZY by utilising the medium and broad-band photometry in a total of 21 filters of JWST/NIRCam and HST from the UNCOVER DR3. The shortest wavelength filter we use is F606W and the longest is F480M.

3. Methods

3.1. Identification

A2744-GDSp-z4 was first recognized as an unusual galaxy in a larger study of morphological properties of high redshift galaxies at $3 < z < 6$ using UNCOVER data in the A2744 field. In that study, we conducted a visual and quantitative morphological classification of galaxies with a photometric redshift of $3 < z < 6$ by dividing the galaxy sample into seven classes: disk only, spheroid only, irregular only, disk + spheroid, disk + irregular, spheroid + irregular and disk + spheroid + irregular. In our visual morphological classification, we identified A2744-GDSp-z4 as a spheroid + disk galaxy i.e. this galaxy contains a central bulge component and a disk. The spiral galaxy shows a grand-design spiral pattern with two well-formed spiral arms (UNCOVER DR3 SUPER catalog id of 42812). We have listed some of the relevant parameters from the catalog for A2744-GDSp-z4 in Table 1.

From the UNCOVER DR3 catalog, we learn that the maximum likelihood photometric redshift of A2744-GDSp-z4 derived via two independent SED modeling codes Prospector and EAZY is ~ 3.88 and ~ 3.90 , respectively. These broadly consistent photometric redshifts likely arise because this galaxy is detected, at high significance, in all JWST/ NIRCam broad-band and medium band filters. It is not well detected in any of the HST/ACS filters where the footprint covers this galaxy, due to the much shallower imaging with the HST. In the F606W HST/ACS filter, the aperture photometry indicates a marginal 3σ detection. Nevertheless, we choose to include this flux in our SED modeling, because as the shortest wavelength filter, it is the only filter that lies slightly blueward of the Lyman- α line for a galaxy at $z \sim 4$. It is not covered in the footprint of any of HST/WFC3 filters. The photometric redshifts obtained with Prospector and EAZY are tightly constrained as seen in Table 1.

There also exists a small spheroid galaxy, near the southern end of the galactic disk. This spheroid galaxy has an UNCOVER DR3 catalog id of 42811 (see the last figure in the bottom panel of Fig. 1). In the UNCOVER DR3 catalog its photometric redshift obtained with Prospector is $z \sim 3.85$. This galaxy also has a robust NIRCam/GRISM spectroscopic redshift of 3.973671 from the All the Little Things (ALT) survey (Naidu et al. 2024) measured using two different emission lines which makes it a candidate satellite galaxy of A2744-GDSp-z4, rather than a chance interloper. Moreover, this spheroid appears to be in the foreground of the disk of A2744-GDSp-z4 further indicating that our object is indeed at a redshift, at least as high, as the spectroscopic redshift of the spheroid galaxy.

3.2. SPS modeling using BAGPIPES

To further verify the photometric redshift of A2744-GDSp-z4, and to measure its properties using the stellar population synthesis (SPS) technique, we carry out spectral energy distribution

Table 1. Basic properties of the A2744-GDSp-z4 galaxy

ID	RA (deg)	Dec (deg)	z_{eazy}	$z_{\text{eazy}_{16}}$ z	$z_{\text{eazy}_{50}}$	$z_{\text{eazy}_{84}}$	$z_{\text{p}_{16}}$	$z_{\text{p}_{50}}$	$z_{\text{p}_{84}}$	R_h (kpc)	R_c (kpc)	mu
42812	3.5237	-30.37241	3.90	3.86	3.89	3.92	3.87	3.90	3.94	3.03	8.14	2.273

Notes. The data presented in this table for A2744-GDSp-z4 are taken from the UNCOVER DR3 catalog with mu being an exception (taken from the UNCOVER DR4 catalog). The catalog ID is the ID of A2744-GDSp-z4 from the UNCOVER DR3 catalog. z_{eazy} is the maximum likelihood photometric redshift derived via EAZY and $z_{\text{eazy}_{16/50/84}}$ are the 16th/50th/84th percentiles of the output photometric redshift posterior from EAZY. $z_{\text{pros}_{16/50/84}}$ are the 16th/50th and 84th percentiles of the Prospector output photometric redshift posterior. R_h and R_c represent the half-light radius and circularised Kron radius of the galaxy in kpc. mu is the strong lensing magnification.

(SED) modeling with another independent state-of-the-art modeling code, Bayesian Analysis of Galaxies for Physical Inference and Parameter Estimation (Bagpipes) (Carnall et al. 2018). Bagpipes provides a framework that allows us to model the observed SEDs of the galaxies by generating synthetic model spectra based on the input parameters. Bagpipes implements SPS models from the 2016 version of the Bruzual & Charlot (2003) models and an initial mass function (IMF) by Kroupa & Boily (2002). Bagpipes allows us to provide the range and priors for the input parameters and set different parametric star formation histories. Bagpipes utilises a nested sampling algorithm PyMultinest (Feroz & Hobson 2008; Feroz et al. 2009, 2019; Buchner et al. 2014) to derive samples from input parameters to generate model SEDs. From the best-fit model, Bagpipes derives joint constraints on photometric redshifts and SPS parameters such as stellar mass, star formation rate (SFR), metallicity, and dust extinction.

We fit two families of star formation histories using Bagpipes – exponentially decaying ($e^{-t/\tau}$) and delayed exponentially decaying star formation ($te^{-t/\tau}$) – to the observed SED, where τ is the timescale of the decrease of the star formation rate. For our modeling, we utilise the aperture photometry of A2744-GDSp-z4 in all JWST/ NIRCam medium and wide-band filters and the F606W filter of HST/ACS from the UNCOVER DR3 catalog. In addition to this, we run EAZY to derive the probability distribution function of the photo-z output posterior. The details of the SED modeling and the list of input parameters provided to EAZY and Bagpipes are given in Appendix A which may be used to reproduce our results.

3.3. Parametric and non-parametric morphology

We perform a two-component bulge-disk decomposition of A2744-GDSp-z4 using GALFIT (Peng et al. 2002, 2010) 4 broadband filters (F200W, F277W, F356W, F444W). While running galfit, we mask out the spheroidal galaxy in the southern part of A2744-GDSp-z4. We present the GALFIT residual in the F277W band in the bottom panel of Fig 1. By modeling and subtracting the light profile of the dominant disk and bulge components, the GALFIT residual allows us to clearly detect the spiral arms.

The morphological nature of high redshift galaxies can be well quantified using standard non-parametric measurements. We calculate concentration, asymmetry, clumpiness (Abraham et al. 1996; Conselice 2003), Gini coefficient (Abraham et al. 2003), and M20 (Lotz et al. 2004) (CASGM) parameters along with multimode-intensity-deviation (MID) statistics (Freeman et al. 2013) for A2744-GDSp-z4 using the Statmorph (Rodriguez-Gomez et al. 2019) software. As inputs, we provide the F444W filter image of A2744-GDSp-z4 along with the segmentation and inverse variance weight map in that filter. We lo-

cate the position of A2744-GDSp-z4 in diagnostic plots of the CASGM parameters and show these plots in Fig 2.

We show 2.5×2.5 arcsec cutouts of A2744-GDSp-z4 in all broadband JWST/NIRCam filters. We have also produced RGB images of this galaxy using filters from the SW and LW channels of the JWST/NIRCam using the software GnuAstro (Akhlaghi & Ichikawa 2015; Akhlaghi 2019b,a). For SW filters we use F090W, F150W, and F200W filters and for LW filters we use F277W, F356W, and F444W filters as our blue, green, and red channels respectively. We show these cutouts and RGB images in Fig 1. We also show a cutout in the F335M filter which contains the H- α + [NII] line complex. In order to locate the spatial distribution of the H- α + [NII] emission in the galactic disk, we produce a RGB image using three medium band filters with F335M as our green channel which contains the line emission and F300M and F360M as our blue and red channels. We present this RGB image and cutout in the F335M filter in Fig 1.

4. Results and discussion

4.1. Robust photometric redshift and SPS outputs from SED modeling

Our SED modeling via Bagpipes yields an output photometric redshift of the galaxy to be $4.036^{+0.008}_{-0.006}$ with tight constraints on the output photo-z posterior (see Fig. A.2). The best-fit model passes through almost all the data points within the error bar. We note that the error bar for the shortest wavelength data point (F606W) is quite large due to the low sensitivity of the HST observation. Only one JWST measurement (F090W) is not consistent with the model, within the error. The strong constraints provided by the numerous, closely-spaced JWST/NIRCam medium-band filters become apparent. The strong blue UV continuum and the presence of several emission lines is as per expectation for a strongly star-forming galaxy. The stellar mass, SFR and the logarithm of the specific star formation rate (sSFR; yr^{-1}) are $\sim 10^{10.15} M_{\odot}$, SFR of $\sim 57.57 M_{\odot} \text{yr}^{-1}$ and ~ -8.42 respectively. We also derive the values of mass-weighted age and A_v . From EAZY, we derive a maximum likelihood redshift of 3.898 with its 16th and 84th percentiles being 3.87 and 3.94 respectively (right panel of Fig.A.1). As with Bagpipes, the best-fit EAZY model, provides an excellent fit to the observed fluxes (left panel of Fig.A.1). The small discrepancy between the Bagpipes and EAZY photometric redshift may be due to the fact that EAZY uses 20 JWST/NIRCam filters and does not use the F606W photometry in the SED modeling. In our Bagpipes modeling we utilise the flux in the F606W HST/ACS filter along with 20 JWST/NIRCam filters as F606W lies blueward to the Lyman- α emission line at $z \sim 4$. We summarize our results from SED modeling via Bagpipes (using two different SFHs) and EAZY in Table 2 for comparison. We have also performed SED modeling for the spheroidal candidate satellite galaxy

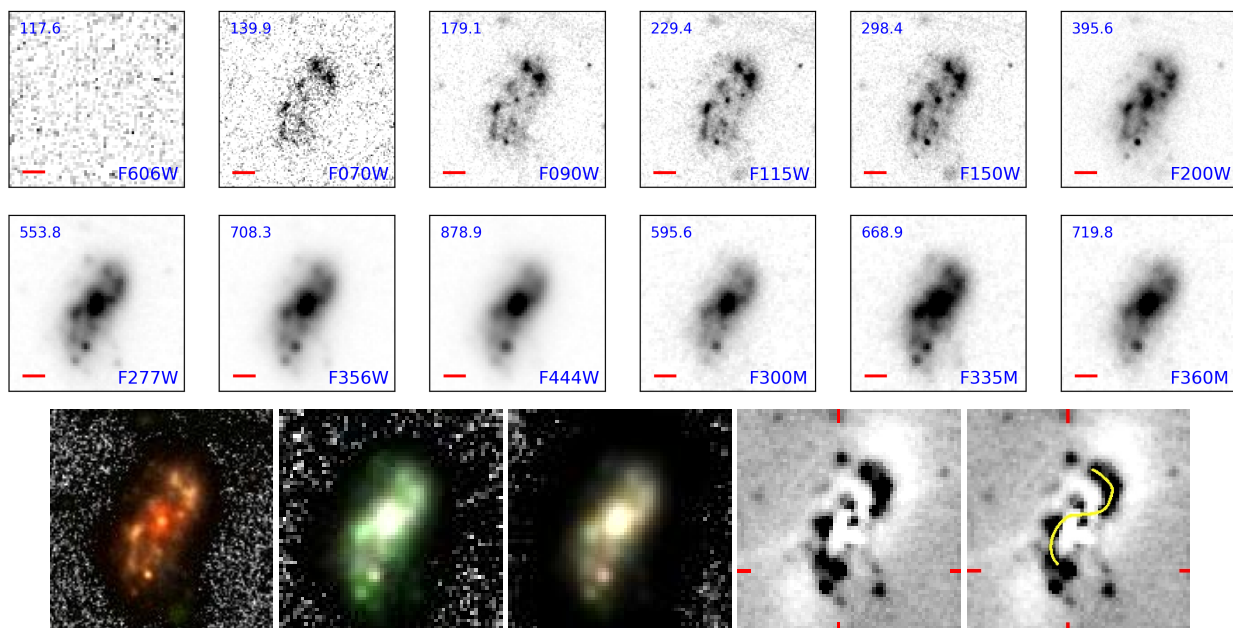


Fig. 1. The two top panels show the grayscale cutouts of A2744-GDSp-z4 in F606 filter (HST/ACS), all JWST/NIRCam broadband filters and three medium band filters F300M, F335M and F360M. The red horizontal bar at the bottom left of each cutout shows 2 kpc scale at the redshift of the galaxy. We also provide the central rest frame wavelength (in nm) for each filter at the top left of each cutout. The F335M filter contains the $H\text{-}\alpha$ + $[\text{NII}]$ line complex. The galactic disk is brighter in the F335M image than the adjacent medium band filter (F300M and F360M) images. The F335M image also shows a bright $H\text{-}\alpha$ + $[\text{NII}]$ region towards the south of the galactic disk which is almost invisible in the F300M and F360M images. The bottom panel shows RGB composite images of the galaxy in this sequence: RGB composite with F200W, F150W, F090W filters, medium band RGB composite with F360M, F335M and F300M filters and RGB image with F444W, F356W and F277W filters. The last two images in the bottom panel show the GALFIT residual in F277W filter and the outline of the spiral arms of the galaxy (yellow curve) superposed on the GALFIT residual, and the red ticks on the x and y axes point to the location of the possible satellite spheroidal galaxy at $z = 3.973671$. All cutouts are 2.5×2.5 arcsec in size. North is on top and East is to the left in all cutouts.

(UNCOVER DR3 ID 42811) and derive a photometric redshift of 3.987 which is in excellent agreement with the spectroscopic galaxy (3.973671) of this galaxy. We emphasize that our results from the SED modeling via EAZY and Bagpipes are broadly consistent with each other for A2744-GDSp-z4.

4.2. Morphology and global physical SPS properties

A2744-GDSp-z4 is a well-formed disk galaxy with a prominent spiral structure at the high redshift of $z \sim 4$. It shows a two-armed spiral structure with a bright central bulge and a large (~ 10 kpc) extended disk. The spiral structure is visible in all JWST/NIRCam broadband and medium-band filters. In the rest frame UV, the star-forming regions in each arm display the familiar beads-on-a-string type structure (Elmegreen & Elmegreen 2014), commonly seen in nearby spirals. In the visible bands, each string appears as an arm and the star-forming regions lose their prominence. From our GALFIT modeling (see Section 3.3), we find that bulge to total luminosity (B/T) ratio increases monotonically from the F200W filter towards the longer wavelength filters. In the longest wavelength broadband filter (F444W) we derive a B/T ratio of ~ 0.18 indicating that this galaxy is an overwhelmingly disk dominated system in rest frame ~ 400 nm to ~ 880 nm.

Using our CASGM statistics, we plot the galaxy on the diagnostic plots of Gini-M20 and log asymmetry vs concentration (Fig 2). At high redshifts Gini-M20 become less reliable to detect galaxy mergers. However, we note that Gini-M20 is sensitive to early phases of a galaxy merger while MID statistics is useful in later stages. Hence using CASGM parameters along with MID statistics provides a robust detection of galaxy mergers (Snyder

et al. 2019; Rose et al. 2024; Freeman et al. 2013). We find that A2744-GSp-z4 lies in the disk region in both plots and has multimode, intensity and deviation values of 0.009, 0.045 and 0.065 respectively. CASGM plots, nearly zero value of deviation and results from our GALFIT analysis strengthens our argument that A2744-GSp-z4 is indeed a well-formed disk at high redshift as seen in Figure 1.

Our SPS modeling with Bagpipes reveals that A2744-GSp-z4 is a massive (stellar mass $\sim 10^{10.15} M_{\odot}$) and vigorously star-forming galaxy with SFR of $\sim 58 M_{\odot} \text{ yr}^{-1}$ and $\log \text{ sSFR} (\text{ yr}^{-1})$ of -8.42 . The large mass, high SFR and sSFR are consistent with its morphological structure which is indicative of a typical star-forming galaxy. The moderate levels of dust extinction ($A_V \sim 0.8$) are not unusual for a starforming galaxy at $z \sim 4$. At this redshift, the $H\text{-}\alpha$ + $[\text{NII}]$ line complex lies within the F335M filter of JWST/NIRCam. In our RGB composite image produced by using three medium band filters (F300M, F335M and F360M), the entire disk, and somewhat more prominently the spiral arms show a green hue due to the detection of $H\text{-}\alpha$ + $[\text{NII}]$ line complex in the green channel (bottom row of Fig. 1). This indicates that the star formation is occurring throughout the disk. We also show the grayscale images of this galaxy in the above three medium band filters (middle panel of Fig. 1). We see a bright $H\text{-}\alpha$ region in the F335M filter image on the southern edge of the disk whereas, it is nearly invisible in the adjacent medium band filters.

We derive the mass weighted age of this galaxy to be 0.228 Gyr. We also determine the time of onset of star formation in this galaxy using a delayed exponential star-formation history model. The onset of star formation occurs approximately 839 Myr after the Big Bang (see Fig. A.3). Hence, this galaxy has

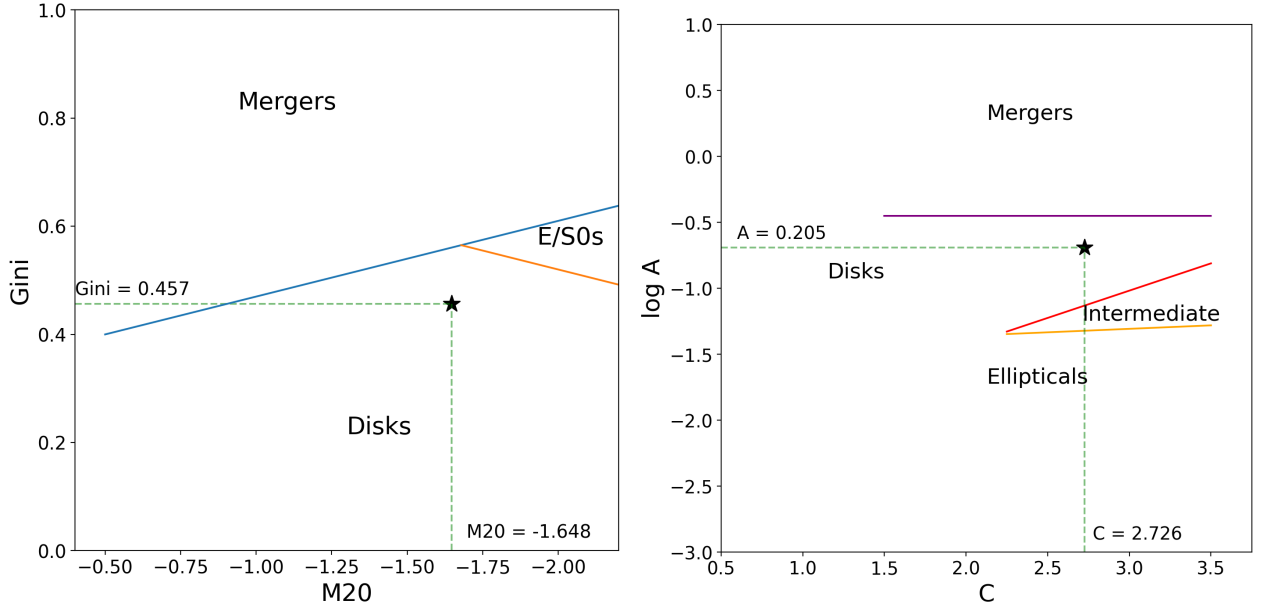


Fig. 2. The left panel shows a plot of the Gini coefficient against the M20 parameter. The lines separating merger, disk, and E/S0 galaxies have been taken from Lotz et al. (2008). The right panel shows the log of the Asymmetry against Concentration. The line separating mergers and disks has been taken from Conselice (2003), where $A = 0.35$. The other two lines separating the population of disk, intermediate, and elliptical galaxies have been taken from Bershady et al. (2000). Exact values are marked in both panels. The value of the smoothness (clumpiness) parameter (not shown in the figure) is 0.014.

Table 2. SPS results from Bagpipes and EAZY

Parameter	Bagpipes(delayed)	Bagpipes(exp)	Eazy
z_{ml}	4.033	4.039	3.898
z_p	4.030 / 4.036 / 4.044	4.034 / 4.043 / 4.056	3.87 / 3.91 / 3.94
mass_p ($\log M_\odot$)	10.14 / 10.15 / 10.16	10.12 / 10.13 / 10.14	10.27, 10.38, 10.47
SFR_p ($M_\odot \text{ yr}^{-1}$)	55.67 / 57.57 / 59.37	61.24 / 63.31 / 65.25	57.77, 59.79, 61.71
sSFR_p	-8.43 / -8.42 / -8.40	-8.39 / -8.36 / -8.34	-8.61, -8.59, -8.58
A_v_p	0.78 / 0.79 / 0.80	0.80 / 0.81 / 0.82	1.01, 1.13, 1.24
MWA_p (Gyr)	0.216 / 0.228 / 0.239	0.154 / 0.162 / 0.170	

Notes. This table shows the SPS properties of derived via two configurations of Bagpipes (exponentially decaying SFH and delayed exponentially decaying SFH) and EAZY. z_{ml} is the maximum likelihood redshift obtained by SED modeling. In other rows, we show, in order, the 16th/50th/84th output posterior percentiles of photometric redshift, stellar mass, SFR, logarithm of sSFR, dust extinction (A_v) and mass-weighted age (MWA). EAZY does not derive the mass weighted age.

assembled a mass of 10 billion solar masses in a few hundred million years and the age of the Universe at this redshift (4.033) is only about 1.5 Gyr. Formation of such a massive spiral disk galaxy at this redshift is not consistent with hierarchical models of galaxy formation (Somerville & Davé 2015).

4.3. Insights into spiral arm formation at high redshift

Before the advent of JWST, the broad consensus in the literature was that galaxies have a highly clumpy structure at $z > 1$ (Conselice et al. 2005). Unstable primordial disks formed by smooth accretion get fragmented into clumpy disks which, in turn, may evolve into spirals. At later epochs, the velocity dispersion of clumpy galaxies decreases and their disks become more stable. These dynamically cold disks can form spiral arms within 1 Gyr provided they do not get destroyed by major mergers (Bournaud et al. 2007; Genzel et al. 2006; Elmegreen et al. 2009a,b; Elmegreen & Elmegreen 2014). Such a formation scenario is consistent with the first appearance of spiral galaxies between redshifts of 1.4 and 1.8 in HST observations (Elmegreen

& Elmegreen 2014). According to a different statistical study by Margalef-Bentabol et al. (2022) in the CANDELS field with HST observations, spiral galaxies appear between the redshifts of 1.5 to 3.

The formation of grand design spiral patterns at high redshifts, in relatively unstable hot disks is not excluded. They could form through perturbations produced by minor galaxy mergers or bar interactions (Elmegreen & Elmegreen 2014; Law et al. 2012). The spiral structures produced by mergers are short-lived and have material arms. Cold disks are required for density waves to emerge, which later form long-lived spiral patterns. One example is the spiral galaxy discovered by Yuan et al. (2017) with a cold disk at $z = 2.54$. Such high redshift cold disks may form spiral arms following QSS Density wave theory.

JWST has begun to unveil substantial disk galaxy populations at $z > 3$ (Kartaltepe et al. 2023; Ferreira et al. 2022; Nelson et al. 2023; Robertson et al. 2023). Rowland et al. (2024) have recently discovered a dynamically cold disk galaxy at $z = 7.3$ with ALMA. In light of these new discoveries, it has been proposed that cold disks were already present in the Universe at redshifts

of $z \sim 3 - 4$ Kuhn et al. (2024). Another study by Kohandel et al. (2024) has also provided evidence for the existence of cold disks at high redshift through simulations and JWST/NIRSpec spectroscopic observations.

The environment density around high redshift spirals may also play a role in driving their structural properties. The high redshift spiral galaxies discovered by Law et al. (2012) and Wu et al. (2022) are located in high-density environments and show ongoing merger signatures. We find that within the projected radial distance of ~ 30 kpc from A2744-GDSp-z4, there are no other sources except for the small candidate satellite galaxy (ID: 42811). A2744-GDSp-z4 sits in a low-density environment and does not display any obvious evidence of ongoing or recent merger activity.

The formation of the spiral patterns may also be driven by a stellar bar within the disk. Huang et al. (2023) have also reported the discovery of a spiral galaxy at $z = 2.467$ whose formation may be bar-driven. A2744-GDSp-z4 has a large bulge and there may be a bar buried within it. Such a bar, if it exists, might be driving the formation of the spiral structure.

How did A2744-GDSp-z4 acquire such a large disk in such a short time? How and when did the grand-design spiral arms emerge? These questions could be answered by investigating the dynamical state of this galaxy with future JWST/NIRSpec IFU observations. Such observations will also provide a spectroscopic redshift. Ascertaining whether the disk of A244-GDSp-z4 is dynamically hot or cold can provide clues into the formation mechanism of the spiral arms, in this intriguing galaxy.

Acknowledgements. R.J. and Y.W. acknowledge the support of the Department of Atomic Energy, Government of India, under project no. 12-R&D-TFR5.02-0700.

Appendix A: SED modeling using Bagpipes and EAZY

A.1. EAZY SED modeling parameters, fitted SED and redshift posterior

In our modeling with EAZY, we use the corr-SFHZ templates (Steinhardt et al. 2023; Carnall et al. 2023), provide a noise floor of 5 percent to account for additional uncertainties with the calibration of JWST data (Boyer et al. 2022), and turn off the priors on the magnitude and UV slope. We set the input redshift range in a grid of 0.01 to 30 with a step size of 0.01. We also do not perform traditional iterative zero-point correction methods as provided in the EAZY documentation. We derive output photometric redshift posterior along with the best-fit SED model and SPS parameters. The output of EAZY modeling is provided in Fig. A.1. The SED of the galaxy is well fitted by the model. The redshift posterior distribution is also narrow and single-peaked.

A.2. Bagpipes SED modeling parameters, fitted model, star formation history and corner plots

We have used the SED modeling Bagpipes to derive joint constraints on the photometric redshift and SPS properties. As input, we provide the ranges of SPS parameters and star formation histories (Section 3). The range and meaning of the input parameters are provided in Table A.1. The rest of the parameters have been kept at their default configuration. We have fitted exponentially decaying and delayed exponentially decaying star formation histories (SFHs). In Fig A.2 and Fig A.3 we provide the output SED fit, one-dimensional posteriors, output SED fit, fitted SFH, and corner plots obtained for the delayed star formation histories.

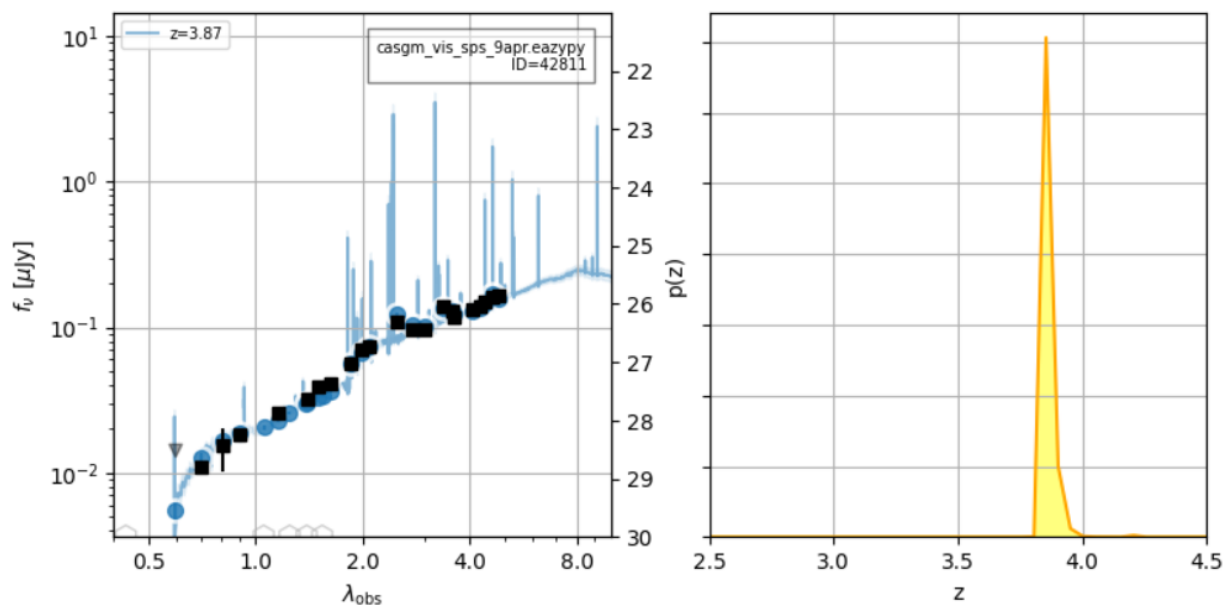


Fig. A.1. The left panel shows the model SED fit obtained by EAZY in blue. The black points are the observed fluxes in the observed frame. The right panel shows the photo- z output posterior (probability distribution function) which is narrow and single-peaked.

Table A.1. Input parameters for SED modeling with Bagpipes

Parameter	Range	Remarks
Redshift	0 - 10	
Stellar mass	7 - 15 $\log M_{\odot}$	log uniform prior
Metallicity	0 - 2.5 Z_{\odot}	
Dust (A_v)	0 - 4	Dust attenuation parameter in V-band (Calzetti dust law)
Dust (Eta)	2	Multiplicative factor on A_v for stars in birth clouds (Charlot & Fall 2000)
Nebular emission	$\log U = -3$	logarithm of the ionization parameter
Age	0.1 - 15 Gyr	Restricted to the age of the Universe at the redshift
τ	0.3 - 10 Gyr	Half-life timescale of the decrease of star formation

Notes. This table shows the SPS properties of derived via two configurations of Bagpipes (exponentially decaying SFH and delayed exponentially decaying SFH) and EAZY. z_{ml} is the maximum likelihood redshift obtained by SED modeling. In other rows, we show, in order, the 16th/50th/84th output posterior percentiles of photometric redshift, stellar mass, SFR, logarithm of sSFR, dust extinction (A_v) and mass-weighted age (MWA). EAZY does not derive the mass weighted age.

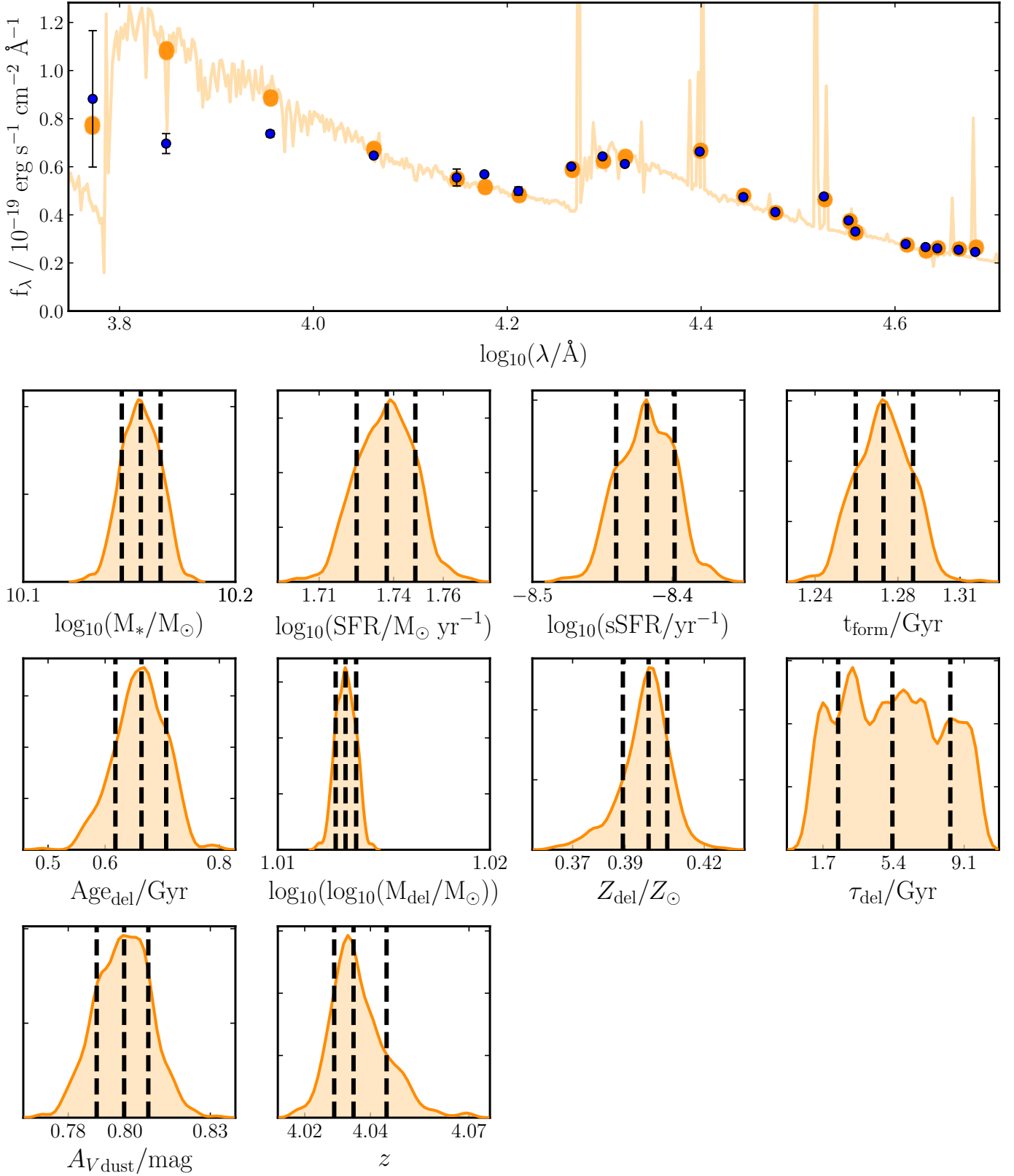


Fig. A.2. In the upper panel, we show the fitted model (in orange) and the observed photometry with error bars as blue points. In the lower panel, we show the 1d posterior of output SPS parameters (labeled on the x-axis) with three black vertical dashed lines indicating the values of the 16th, 50th and 84th percentile of the output posterior probability distribution of each parameter.

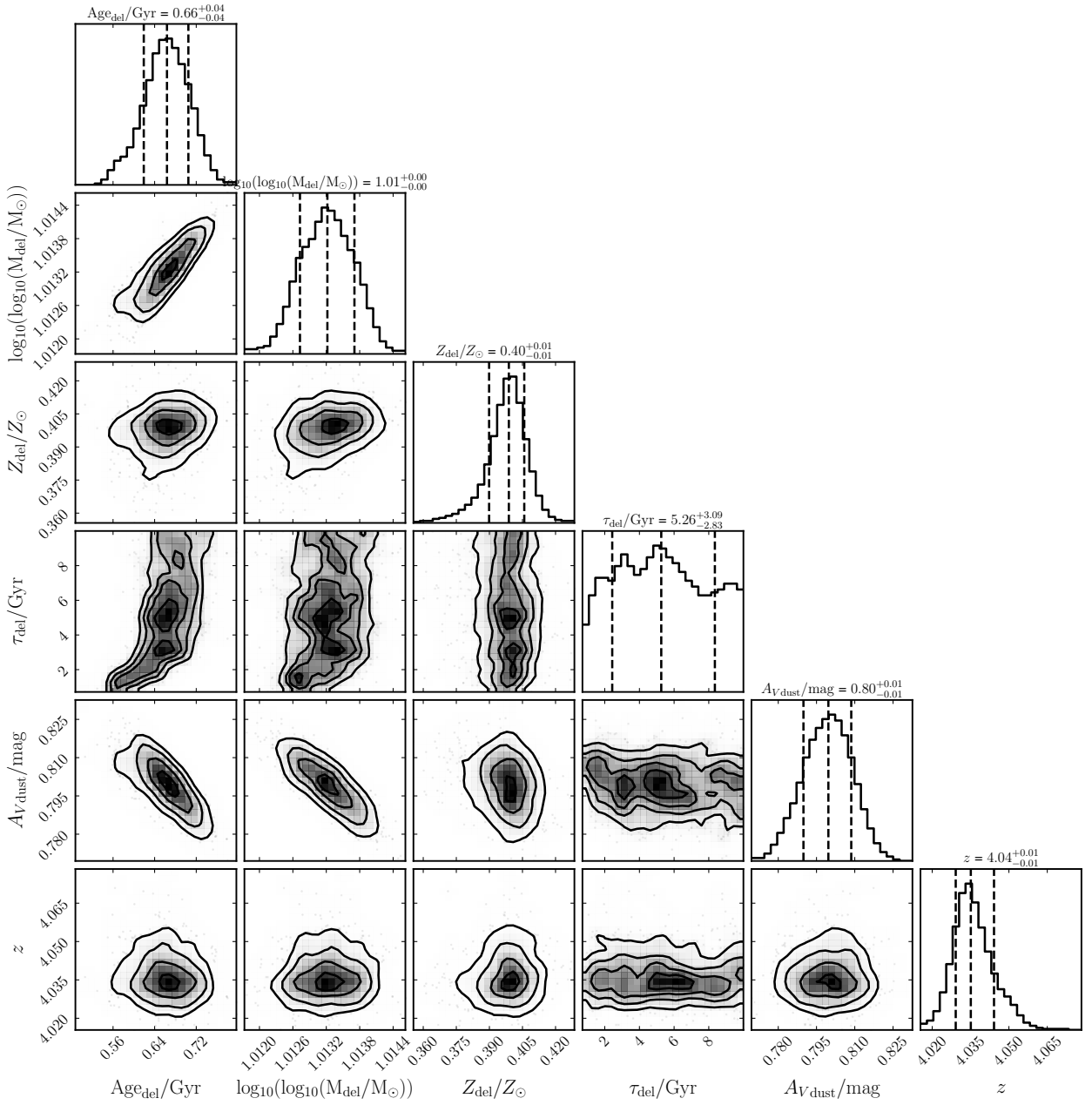
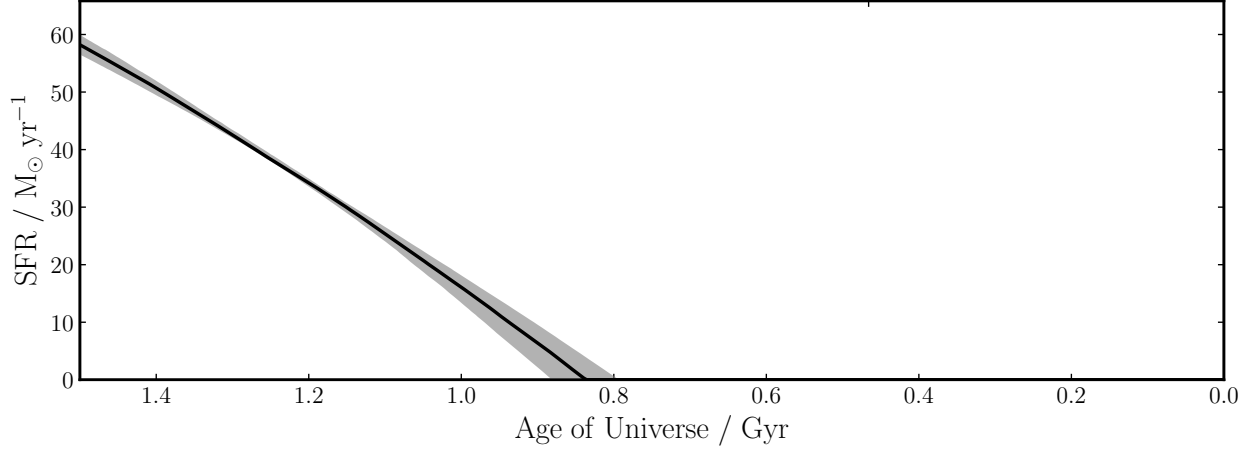


Fig. A.3. In the upper panel of this figure, we show the delayed exponential star formation history fitted by Bagpipes to the observed photometry of the galaxy. In the lower panel, we show the corner plots for the output parameters such as mass, redshift, and A_V .

References

- Abraham, R. G., Tanvir, N. R., Santiago, B. X., et al. 1996, *MNRAS*, 279, L47
- Abraham, R. G., van den Bergh, S., & Nair, P. 2003, *ApJ*, 588, 218
- Akhlaghi, M. 2019a, arXiv e-prints, arXiv:1909.11230
- Akhlaghi, M. 2019b, *ASPC*, 521, 299
- Akhlaghi, M. & Ichikawa, T. 2015, *ApJS*, 220, 1
- Bershady, M. A., Jangren, A., & Conselice, C. J. 2000, *The Astronomical Journal*, 119, 2645
- Bezanson, R., Labbé, I., Whitaker, K. E., et al. 2022, arXiv e-prints, arXiv:2212.04026
- Bournaud, F., Elmegreen, B. G., & Elmegreen, D. M. 2007, *The Astrophysical Journal*, 670, 237
- Boyer, M. L., Anderson, J., Gennaro, M., et al. 2022, *Research Notes of the AAS*, 6, 191
- Brammer, G. B., van Dokkum, P. G., & Coppi, P. 2008, *ApJ*, 686, 1503
- Bruzual, G. & Charlot, S. 2003, *Monthly Notices of the Royal Astronomical Society*, 344, 1000
- Buchner, J., Georgakakis, A., Nandra, K., et al. 2014, *Astronomy & Astrophysics*, 564, A125
- Carnall, A. C., Begley, R., McLeod, D. J., et al. 2023, *MNRAS*, 518, L45
- Carnall, A. C., McLure, R. J., Dunlop, J. S., & Davé, R. 2018, *Monthly Notices of the Royal Astronomical Society*, 480, 4379–4401
- Charlot, S. & Fall, S. M. 2000, *ApJ*, 539, 718
- Conselice, C. J. 2003, *ApJS*, 147, 1
- Conselice, C. J., Blackburne, J. A., & Papovich, C. 2005, *ApJ*, 620, 564
- Costantin, L., Pérez-González, P. G., Guo, Y., et al. 2023, *Nature*, 623, 499
- Elmegreen, B. G., Elmegreen, D. M., Fernandez, M. X., & Lemonias, J. J. 2009a, *The Astrophysical Journal*, 692, 12
- Elmegreen, D. M. & Elmegreen, B. G. 2014, *ApJ*, 781, 11
- Elmegreen, D. M., Elmegreen, B. G., Marcus, M. T., et al. 2009b, *The Astrophysical Journal*, 701, 306
- Feroz, F. & Hobson, M. P. 2008, *Monthly Notices of the Royal Astronomical Society*, 384, 449
- Feroz, F., Hobson, M. P., & Bridges, M. 2009, *Monthly Notices of the Royal Astronomical Society*, 398, 1601
- Feroz, F., Hobson, M. P., Cameron, E., & Pettitt, A. N. 2019, *The Open Journal of Astrophysics*, 2
- Ferreira, L., Adams, N., Conselice, C. J., et al. 2022, *The Astrophysical Journal Letters*, 938, L2
- Ferreira, L., Conselice, C. J., Sazonova, E., et al. 2023, *ApJ*, 955, 94
- Freeman, P. E., Izbicki, R., Lee, A. B., et al. 2013, *Monthly Notices of the Royal Astronomical Society*, 434, 282
- Fudamoto, Y., Inoue, A. K., & Sugahara, Y. 2022, *ApJ*, 938, L24
- Furtak, L. J., Zitrin, A., Weaver, J. R., et al. 2023, *MNRAS*, 523, 4568
- Genzel, R., Tacconi, L. J., Eisenhauer, F., et al. 2006, *Nature*, 442, 786
- Huang, S., Kawabe, R., Kohno, K., et al. 2023, *The Astrophysical Journal Letters*, 958, L26
- Jacobs, C., Glazebrook, K., Calabrò, A., et al. 2023, *ApJ*, 948, L13
- Johnson, B. D., Leja, J., Conroy, C., & Speagle, J. S. 2021, *ApJS*, 254, 22
- Kartaltepe, J. S., Rose, C., Vanderhoof, B. N., et al. 2023, *The Astrophysical Journal Letters*, 946, L15
- Kohandel, M., Pallottini, A., Ferrara, A., et al. 2024, *A&A*, 685, A72
- Kroupa, P. & Boily, C. M. 2002, *MNRAS*, 336, 1188
- Kuhn, V., Guo, Y., Martin, A., et al. 2024, *The Astrophysical Journal Letters*, 968, L15
- Labbé, I., van Dokkum, P., Nelson, E., et al. 2023, *Nature*, 616, 266
- Law, D. R., Shapley, A. E., Steidel, C. C., et al. 2012, *Nature*, 487, 338–340
- Lin, C. C. & Shu, F. H. 1964, *ApJ*, 140, 646
- Lotz, J. M., Davis, M., Faber, S. M., et al. 2008, *ApJ*, 672, 177
- Lotz, J. M., Primack, J., & Madau, P. 2004, *AJ*, 128, 163
- Margalef-Bentabol, B., Conselice, C. J., Haeussler, B., et al. 2022, *Monthly Notices of the Royal Astronomical Society*, 511, 1502
- Naidu, R. P., Matthee, J., Kramarenko, I., et al. 2024, arXiv e-prints, arXiv:2410.01874
- Nelson, E. J., Suess, K. A., Bezanson, R., et al. 2023, *ApJ*, 948, L18
- Peng, C. Y., Ho, L. C., Impey, C. D., & Rix, H.-W. 2002, *AJ*, 124, 266
- Peng, C. Y., Ho, L. C., Impey, C. D., & Rix, H.-W. 2010, *AJ*, 139, 2097
- Rawat, A., Wadadekar, Y., & De Mello, D. 2009, *ApJ*, 695, 1315
- Robertson, B. E., Tacchella, S., Johnson, B. D., et al. 2023, *ApJ*, 942, L42
- Rodríguez-Gomez, V., Snyder, G. F., Lotz, J. M., et al. 2019, *MNRAS*, 483, 4140
- Rose, C., Kartaltepe, J. S., Snyder, G. F., et al. 2024, arXiv e-prints, arXiv:2407.21279
- Rowland, L. E., Hodge, J., Bouwens, R., et al. 2024, arXiv e-prints, arXiv:2405.06025
- Sellwood, J. A. 2014, *Reviews of Modern Physics*, 86, 1
- Snyder, G. F., Rodríguez-Gomez, V., Lotz, J. M., et al. 2019, *Monthly Notices of the Royal Astronomical Society*, 486, 3702
- Somerville, R. S. & Davé, R. 2015, *ARA&A*, 53, 51
- Steinhardt, C. L., Kokorev, V., Rusakov, V., Garcia, E., & Sneppen, A. 2023, *The Astrophysical Journal Letters*, 951, L40
- Suess, K. A., Weaver, J. R., Price, S. H., et al. 2024, arXiv e-prints, arXiv:2404.13132
- Toomre, A. 1977, *ARA&A*, 15, 437
- Toomre, A. 1981, in *Structure and Evolution of Normal Galaxies*, ed. S. M. Fall & D. Lynden-Bell, 111–136
- Tsukui, T. & Iguchi, S. 2021, *Science*, 372, 1201
- Tsukui, T., Wisnioski, E., Bland-Hawthorn, J., et al. 2024, *MNRAS*, 527, 8941
- Tsukui, T., Wisnioski, E., Krumholz, M. R., & Battisti, A. 2023, *MNRAS*, 523, 4654
- Wang, B., Leja, J., Labbé, I., et al. 2024, *ApJS*, 270, 12
- Weaver, J. R., Cutler, S. E., Pan, R., et al. 2024, *ApJS*, 270, 7
- Wu, Y., Cai, Z., Sun, F., et al. 2022, *The Astrophysical Journal Letters*, 942, L1
- Yuan, T., Richard, J., Gupta, A., et al. 2017, *ApJ*, 850, 61